

Classical variational simulation of the Quantum Approximate Optimization Algorithm

Matija Medvidović

Center for Computational Quantum Physics, Flatiron Institute,

162 5th Avenue, New York, NY 10010, USA and

Department of Physics, Columbia University, New York 10027, USA

Giuseppe Carleo

Institute of Physics, École Polytechnique Fédérale de Lausanne (EPFL), CH-1015 Lausanne, Switzerland

We introduce a method to classically simulate quantum circuits consisting of several layers of parameterized gates, a key component of many variational quantum algorithms suitable for near-term quantum computers. The classical simulation approach we adopt is based on a neural-network quantum state parameterization of the many-qubit wave function. As a specific example, we focus on alternating layered ansatz states that are relevant for the Quantum Approximate Optimization Algorithm (QAOA). The method complements current state-of-the-art exact simulations in that its validity is not strongly constrained by qubit count, topologies or circuit depth but rather by choice of QAOA angles. We study the MaxCut problem on 3-regular graphs for both 20 and 54 qubit systems at QAOA depths of 1, 2 and 4. For the largest circuits simulated we reach 20 layers of independent gates (depth) without requiring large-scale computational resources. When available, we compare the obtained states with outputs of exact simulators and find good approximations for both the cost function values and state vectors. For larger number of qubits, our approach can be used to provide accurate simulations of QAOA at previously unexplored regions of its parameter space, and to benchmark the next generation of experiments in the Noisy Intermediate-Scale Quantum (NISQ) era.

I. INTRODUCTION

The past decade has seen a fast development of quantum technologies and the achievement of an unprecedented level of control in quantum hardware [1], opening to demonstrations of quantum computing applications for practical uses. Near-term applications however face some of the limitations intrinsic to the current generation of quantum computers, often referred to as Noisy Intermediate-Scale Quantum (NISQ) hardware [2]. In this regime, a limited qubits count and the absence of quantum error correction, constrain the kind of applications that can be successfully realized. Despite these limitations, hybrid classical-quantum algorithms [3–6] have been identified as the ideal candidates to assess the first possible advantage of quantum computing in practical applications.

The Quantum Approximate Optimization Algorithm (QAOA) [5] is a notable example of variational quantum algorithm with prospects of quantum speedup on near-term devices. Devised to take advantage of quantum effects to solve combinatorial optimization problems, it has been extensively theoretically characterized [7–12], and also experimentally realized on state-of-the-art NISQ hardware [13]. While the general presence of quantum advantage in quantum optimization algorithms remains an open question [14–16], QAOA has gained popularity as a quantum hardware benchmark [17–20]. As its desired output is essentially a classical state, the question arises whether a specialized classical algorithm can efficiently simulate it [21], at least near the variational optimum.

In this paper, we use a classical variational parameter-

ization of the many-qubit state based on Neural Network Quantum States (NQS) [22] and extend the method of Ref. [23] to simulate QAOA. This approach trades the need for exact *brute force* exponentially scaling classical summation with an approximate, yet accurate, classical variational description of the quantum circuit. In turn, we obtain an heuristic classical method that can significantly expand the possibilities to simulate NISQ-era quantum optimization algorithms. We successfully simulate the Max-Cut QAOA circuit [5, 7, 13] for 54 qubits at depth $p = 4$ and use the method to perform a variational parameter sweep on a 1D cut of the parameter space. The method is contrasted with state-of-the-art classical simulations based on low-rank Clifford group decompositions [21], whose complexity is exponential in the number of non-Clifford gates. Instead, limitations of the approach are discussed in terms of the QAOA parameter space and its relation to different initializations of the stochastic optimization method used in this work.

II. METHODS

In this section, we discuss the theoretical foundations of QAOA, defining relevant operators and the cost function. In addition, we discuss Restricted Boltzmann Machines, a class of NQS we use for quantum simulation. Unitary gate application is discussed as well as stochastic optimization it entails.

A. Quantum Approximate Optimization Algorithm for the MaxCut problem

The Quantum Approximate Optimization Algorithm (QAOA) [5, 8] is a variational quantum algorithm for approximately solving discrete combinatorial optimization problems. In this work, we study a quadratic cost function associated with a MaxCut problem on graphs.

If we consider a graph G and denote the set of its edges by $E(G)$, the MaxCut of the graph G is defined by the following operator:

$$\mathcal{C} = \sum_{i,j \in E(G)} w_{ij} Z_i Z_j, \quad (1)$$

where w_{ij} are the edge weights. The classical bitstring \mathcal{B} that minimizes $\langle \mathcal{B} | \mathcal{C} | \mathcal{B} \rangle$ is the graph partition with the maximum cut. QAOA approximates such a quantum state through a quantum circuit of predefined depth p :

$$|\gamma, \beta\rangle = U_B(\beta_p) U_C(\gamma_p) \cdots U_B(\beta_1) U_C(\gamma_1) |+\rangle, \quad (2)$$

where $|+\rangle$ is a symmetric superposition of all computational basis states: $|+\rangle = H^{\otimes N} |0\rangle^{\otimes N}$ for N qubits. The set of $2p$ real numbers γ_i and β_i for $i = 1 \dots p$ define the variational parameters to be optimized over by an external classical optimizer. Unitary gates U_B and U_C are defined as follows:

- $U_C(\gamma) = e^{-i\gamma\mathcal{C}} = \prod_{i,j \in E(G)} e^{-i\gamma w_{ij} Z_i Z_j}$
- $U_B(\beta) = \prod_{i \in G} e^{-i\beta X_i}$

Optimal variational parameters γ and β are then found through an outer-loop classical optimizer of the following quantum expectation value:

$$C(\gamma, \beta) = \langle \gamma, \beta | \mathcal{C} | \gamma, \beta \rangle \quad (3)$$

In this work we consider 3-regular graphs with all weights w_{ij} set to unity at QAOA depths of $p = 1, 2, 4$. At $p = 1$, we base our parameter choices on the exact position of global optimum that is easily accessible through Theorem 1.

Theorem 1 *For an arbitrary graph G , the QAOA cost function for the MaxCut problem given in Eq. 3 takes the form*

$$\begin{aligned} C(\gamma, \beta) = & \\ & \frac{1}{2} \sum_{\langle k, l \rangle} \left[\sin(4\beta) \sin(2\gamma) (\cos^{q_k}(2\gamma) + \cos^{q_l}(2\gamma)) + \right. \\ & \left. + \sin^2(2\beta) \cos^{q_k+q_l-2\Delta_{kl}}(2\gamma) (1 - \cos^{\Delta_{kl}}(4\gamma)) \right] \end{aligned} \quad (4)$$

at $p = 1$. Here, $q_k + 1$ and $q_l + 1$ are degrees of vertices k and l and Δ_{kl} is the number of common neighbors between those vertices.

An almost identical theorem can be found in [7] but our expression differs in numerical prefactors and signs that cannot be attributed to parameter rescaling. The complete derivation can be found in Appendix C.

For $p = 2$ and $p = 4$, we resort to direct numerical evaluation of the cost function as given in Eq. 1 from either the complete state vector of the system (number of qubits permitting) or from importance-sampling the output state as represented by a Restricted Boltzmann Machine. For all p , we find the optimal angles using Adam [24] with either numerical or exact gradients.

B. Restricted Boltzmann Machines as Quantum States

Consider a quantum system consisting of N qubits. The Hilbert space is spanned by the computational basis $\{|\mathcal{B}\rangle : \mathcal{B} \in \{0, 1\}^N\}$ of classical bit strings $\mathcal{B} = (B_1, \dots, B_N)$. A general state can be expanded in this basis as $|\psi\rangle = \sum_{\mathcal{B}} \psi(\mathcal{B}) |\mathcal{B}\rangle$. The convention $Z_i |\mathcal{B}\rangle = (-1)^{B_i} |\mathcal{B}\rangle$ is adopted. We use a neural-network representation of the many-body wavefunction $\psi(\mathcal{B})$ associated with this system, and specifically adopt a shallow network of the Restricted Boltzmann Machine (RBM) type: [25–27]

$$\begin{aligned} \psi(\mathcal{B}) \approx \psi_{\theta}(\mathcal{B}) \equiv & \exp \left(\sum_{j=1}^N a_j B_j \right) \cdot \\ & \cdot \prod_{k=1}^{N_h} \left[1 + \exp \left(b_k + \sum_{j=1}^{N_v} W_{jk} B_j \right) \right]. \end{aligned} \quad (5)$$

The RBM provides a classical variational representation of the quantum state [22], and is parametrized by a set of complex parameters $\theta = \{\mathbf{a}, \mathbf{b}, W\}$ – visible biases $\mathbf{a} = (a_1, \dots, a_N)$, hidden biases $\mathbf{b} = (b_1, \dots, b_{N_h})$ and weights $W = (W_{j,k} : j = 1 \dots N, k = 1 \dots N_h)$. The complex-valued ansatz given in Eq. 5 is, in general, not normalized.

We note that the N -qubit $|+\rangle$ state required for initializing QAOA can always be exactly implemented by setting all variational parameters to 0. That choice ensures that the wavefunction ansatz given in Eq. 5 is constant across all computational basis states, as required. Subsequent unitary gate application is discussed in the following sections.

1. Exact gate application to RBMs

In what follows, a generic quantum circuits composed of local gates is considered. The advantage of using the ansatz given in Eq. 5 as an N -qubit state is that a subset of one- and two-qubit gates can be exactly implemented as mappings between different sets of variational parameters $\theta \mapsto \theta'$. In general, such mapping corresponding to

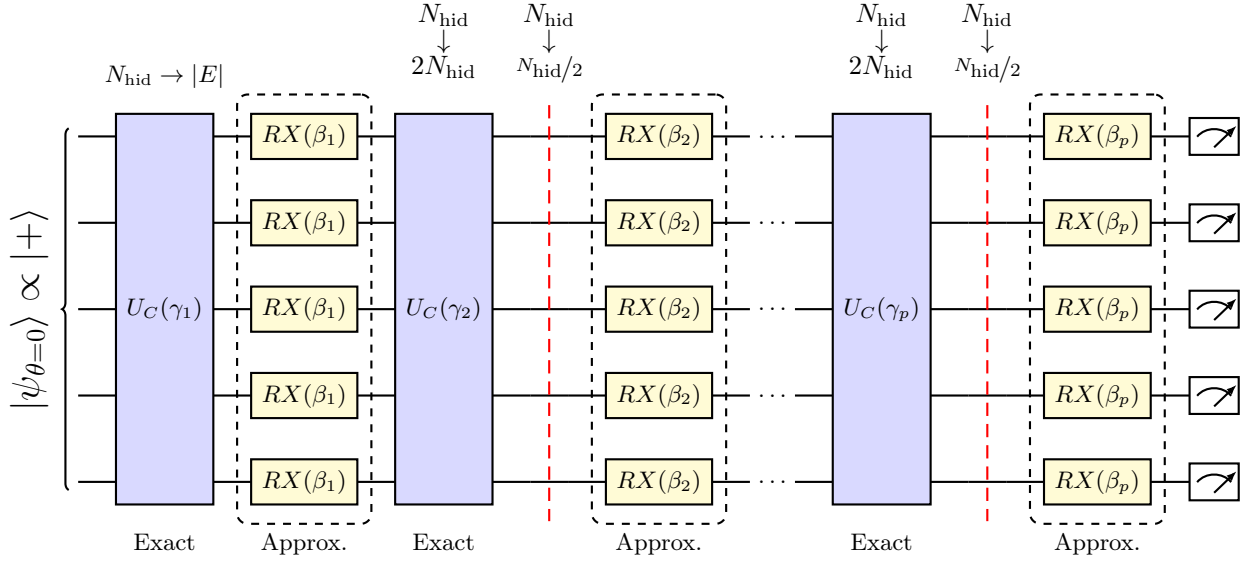


FIG. 1. A schematic representation of the QAOA circuit and our approach to simulating it. The input state is trivially initialized to $|+\rangle$. Next, at each p , the exchange of exactly (U_C , Sec. II B 1) and approximately ($RX(\beta) = e^{-i\beta X}$, Sec. II B 2) applicable gates is labeled. As noted in the main text, each (exact) application of the U_C gate leads to an increase in the number of hidden units by $|E|$ (the number of edges in the graph). In order to keep that number constant, we compress the number of hidden units (Sec. II C), indicated by red dashed lines after each U_C gate. The compression is repeated at each layer after the first, halving the number of hidden units each time.

an abstract gate \mathcal{G} is found as the solution of the following nonlinear equation:

$$\langle \mathcal{B} | \psi_{\theta'} \rangle = C \langle \mathcal{B} | \mathcal{G} | \psi_{\theta} \rangle , \quad (6)$$

for all bitstrings \mathcal{B} and any constant C , if a solution exists. For example, consider the Pauli Z gate acting on qubit i . In that case, Eq. 6 reads $e^{a'_i B_i} = C(-1)^{B_i} e^{a_i B_i}$ after trivial simplification. The solution is $a'_i = a_i + i\pi$ for $C = 1$, with all other parameters remaining unchanged. Such replacement rules for all three Pauli gates can be found in Table I.

| | C | \mathbf{a}' | \mathbf{b}' | W' |
|-------|----------------|----------------------|-----------------------|---------------------|
| X_i | a_i | $a'_i = -a_i$ | $b'_k = b_k + W_{ik}$ | $W'_{ik} = -W_{ik}$ |
| Y_i | $a_i + i\pi/2$ | $a'_i = -a_i + i\pi$ | $b'_k = b_k + W_{ik}$ | $W'_{ik} = -W_{ik}$ |
| Z_i | 1 | $a_i + i\pi$ | No change | No change |

TABLE I. Parameter replacement rules for applying Pauli gates to RBMs.

In addition, one can exactly implement a subset of two-qubit gates by introducing an additional hidden unit coupled only to the two qubits in question. Labeling the new unit by c , we can implement the RZZ gate relevant for QAOA. The gate is given as $RZZ(\phi) = e^{-i\phi Z_i Z_j} \propto \text{diag}(1, e^{i\phi}, e^{i\phi}, 1)$ up to a global phase. The replacement rules read:

$$\begin{aligned} W_{ic} &= -2\mathcal{A}(\phi), & W_{jc} &= 2\mathcal{A}(\phi) \\ a_i &\rightarrow a_i + \mathcal{A}(\phi), & a_j &\rightarrow a_j - \mathcal{A}(\phi), \end{aligned} \quad (7)$$

where $\mathcal{A}(\phi) = \text{Arccosh}(e^{i\phi})$ and $C = 2$. Derivations of replacement rules for these and other gates can be found in Appendix A.

2. Approximate gate application to RBMs by stochastic optimization

Not all gates can be applied through solving Eq. 6. Most notably, gates that form superpositions belong in this category, including $U_B(\beta) = \prod_i e^{-i\beta X_i}$ required for running QAOA. This happens simply because a linear combination of two or more RBMs cannot be exactly represented by a single new RBM through a simple variational parameter change. To simulate those gates, we employ a variational stochastic optimization scheme.

We take $\mathcal{D}(\phi, \psi) = 1 - F(\phi, \psi)$ as a measure of distance between two arbitrary quantum states $|\phi\rangle$ and $|\psi\rangle$, where $F(\phi, \psi)$ is the usual quantum fidelity:

$$F(\phi, \psi) = \frac{|\langle \phi | \psi \rangle|^2}{\langle \phi | \phi \rangle \langle \psi | \psi \rangle} , \quad (8)$$

In order to find variational parameters θ which approximate a target state $|\phi\rangle$ well ($|\psi_{\theta}\rangle \approx |\phi\rangle$, up to a normalization constant), we minimize $\mathcal{D}(\psi_{\theta}, \phi)$ using a gradient-based optimizer. In this work we use the Stochastic Re-configuration (SR) [28] algorithm to achieve that goal. To that end, we write $\mathcal{D}(\psi_{\theta}, \phi)$ as an expectation value

Algorithm 1: Target state approximation with an RBM

Input: Initial parameters θ , target state ϕ , target fidelity tolerance tol , learning rate η
Result: Parameters $\theta' = \{\mathbf{a}', \mathbf{b}', W'\}$ such that $|\psi_{\theta'}\rangle \approx |\phi\rangle$
 $\partial_k \ln F \leftarrow 0 ; S_{kl} \leftarrow 0 ; \theta' \leftarrow \theta ;$
while $F < 1 - \text{tol}$ **do**
| Generate samples $\mathcal{B}_\psi \sim |\psi_{\theta'}|^2$ and $\mathcal{B}_\phi \sim |\phi|^2$ using MCMC;
| **foreach** \mathcal{B} in \mathcal{B}_ψ **do** evaluate and store $\psi_{\theta'}(\mathcal{B})$, $\phi(\mathcal{B})$ and $\mathcal{O}_k(\mathcal{B})$ for all parameters ;
| **foreach** \mathcal{B} in \mathcal{B}_ϕ **do** evaluate and store $\psi_{\theta'}(\mathcal{B})$ and $\phi(\mathcal{B})$;
| evaluate and set $F \leftarrow \text{Re} \left\{ \left\langle \frac{\phi(\mathcal{B})}{\psi(\mathcal{B})} \right\rangle_{\mathcal{B} \sim \mathcal{B}_\psi} \left\langle \frac{\psi(\mathcal{B})}{\phi(\mathcal{B})} \right\rangle_{\mathcal{B} \sim \mathcal{B}_\phi} \right\} ;$
| **foreach** k **do** evaluate and set $\partial_k \ln F \leftarrow \langle \mathcal{O}_k^* \rangle_{\mathcal{B} \sim \mathcal{B}_\psi} - \left\langle \frac{\phi}{\psi_\theta} \mathcal{O}_k^* \right\rangle_{\mathcal{B} \sim \mathcal{B}_\psi} / \left\langle \frac{\phi}{\psi_\theta} \right\rangle_{\mathcal{B} \sim \mathcal{B}_\psi} ;$
| **foreach** k, l **do** evaluate and set $S_{kl} \leftarrow \langle \mathcal{O}_k^\dagger \mathcal{O}_l \rangle_{\psi_\theta} - \langle \mathcal{O}_k^\dagger \rangle_{\psi_\theta} \langle \mathcal{O}_l \rangle_{\psi_\theta} ;$
| solve linear system $\sum_l S_{kl} \Delta_l = F \times \partial_k \ln F$;
| **foreach** k **do** $\theta'_k \leftarrow \theta'_k - \eta \Delta_k$;
end
return θ'

of an effective hamiltonian H_{eff}^ϕ :

$$\mathcal{D}(\psi_\theta, \phi) = \frac{\langle \psi_\theta | H_{\text{eff}}^\phi | \psi_\theta \rangle}{\langle \psi_\theta | \psi_\theta \rangle} \quad (9)$$

where

$$H_{\text{eff}}^\phi = \mathbb{1} - \frac{|\phi\rangle\langle\phi|}{\langle\phi|\phi\rangle} \quad (10)$$

We call the hermitian operator given in Eq. 10 a "hamiltonian" only because the target quantum state $|\psi\rangle$ is encoded into it as the eigenstate corresponding to the smallest eigenvalue. Our optimization scheme focuses on finding small parameter updates Δ_k that locally approximate the action of the imaginary time evolution operator associated with H_{eff}^ϕ , thus filtering out the target state:

$$|\psi_{\theta+\Delta}\rangle \stackrel{!}{=} C e^{-\eta H} |\psi_\theta\rangle, \quad (11)$$

where C is an arbitrary constant included because our variational states (Eq. 5) are not normalized. Choosing both η and Δ to be small, one can expand both sides to linear order in those variables and solve the resulting linear system for all components of Δ , after eliminating C first. After some simplification, one arrives at the following parameter at each loop iteration (indexed with t):

$$\theta_k^{(t+1)} = \theta_k^{(t)} - \eta \sum_l S_{kl}^{-1} \frac{\partial \mathcal{D}}{\partial \theta_l^*}, \quad (12)$$

where stochastic estimations of gradients of the cost function $\mathcal{D}(\psi_\theta, \phi)$ can be obtained through samples from $|\psi_\theta|^2$ at each loop iteration through:

$$\frac{\partial \mathcal{D}}{\partial \theta_k^*} = \left\langle \mathcal{O}_k^\dagger H_{\text{eff}}^\phi \right\rangle_{\psi_\theta} - \left\langle \mathcal{O}_k^\dagger \right\rangle_{\psi_\theta} \left\langle H_{\text{eff}}^\phi \right\rangle_{\psi_\theta}. \quad (13)$$

Here, \mathcal{O}_k is defined as a diagonal operator in the computational basis such that $\langle \mathcal{B}' | \mathcal{O}_k | \mathcal{B} \rangle = \frac{\partial \ln \psi_\theta}{\partial \theta_k} \delta_{\mathcal{B}' \mathcal{B}}$.

Averages over ψ_θ are commonly defined as $\langle \cdot \rangle_\psi \equiv \langle \psi | \cdot | \psi \rangle / \langle \psi | \psi \rangle$. Furthermore, the S -matrix appearing in Eq. 12 reads:

$$S_{kl} = \left\langle \mathcal{O}_k^\dagger \mathcal{O}_l \right\rangle_{\psi_\theta} - \left\langle \mathcal{O}_k^\dagger \right\rangle_{\psi_\theta} \left\langle \mathcal{O}_l \right\rangle_{\psi_\theta}, \quad (14)$$

and corresponds to the Quantum Geometric Tensor or Quantum Fisher Information (also see Ref. [29] for a detailed description and connection with the natural gradient method in classical machine learning [30]).

Exact computations of averages over N qubit states ψ_θ and ϕ at each optimization step range from impractical to intractable, even for moderate N . Therefore, we evaluate those averages by importance-sampling the probability distributions associated with the variational ansatz $|\psi_\theta|^2$ and the target state $|\phi|^2$ at each optimization step t . All of the above expectation values are evaluated using Markov Chain Monte Carlo (MCMC) [31, 32] sampling with basic single-spin flip local updates. An overview of the sampling method is provided in Appendix D.

Furthermore, we note that the expression

$$F(\phi, \psi) = \left\langle \frac{\phi(\mathcal{B})}{\psi(\mathcal{B})} \right\rangle_\psi \left\langle \frac{\psi(\mathcal{B})}{\phi(\mathcal{B})} \right\rangle_\phi, \quad (15)$$

contained in Eq. B2 is the stochastic estimator of fidelity between states ψ_θ and ϕ , useful for keeping track of optimizer progress. Further details about the optimization procedure can be found in Appendix B.

The above-described procedure can be used to try to approximate any state ϕ that one can sample. Since $U_C(\gamma)$ gates required for QAOA implementation can be exactly applied within our RBM framework, we require the described optimization procedure for applying $U_B(\beta)$. We achieve this by being able to evaluate

$$\begin{aligned} |\phi\rangle &\equiv e^{-i\beta X_i} |\psi_\theta\rangle = \\ &= \cos \beta |\psi_\theta\rangle - i \sin \beta (X_i |\psi_\theta\rangle) \end{aligned} \quad (16)$$

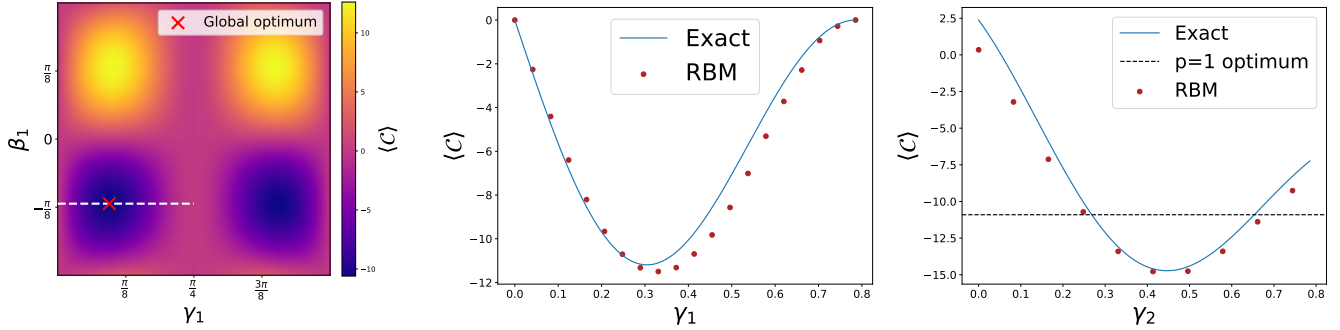


FIG. 2. **Left:** The exact variational QAOA landscape at $p = 1$ of a random 20-qubit instance of a 3-regular graph is presented, calculated using Theorem 1. The optimum was found using a gradient-based optimizer [24] and marked. The restricted cut along the constant- β line and at optimal γ is more closely studied in the center panel. **Center:** RBM-based output wavefunctions are contrasted with exact results. **Right:** A similar variational landscape cut is presented at $p = 2$. Optimal $p = 2$ QAOA parameters are calculated using numerical derivatives and a gradient-based optimizer. Parameters γ_1 , β_1 and β_2 are fixed at their optimal values while the cost function γ_2 -dependence is investigated. We note that our approach is able to accurately reproduce the increased proximity to the combinatorial optimum associated with increasing QAOA depth p .

for each individual qubit indexed by i . The wavefunction associated with the state $X_i|\psi_\theta\rangle$ in Eq. 16 is available for sampling through the parameter replacement rules given in Table I. We repeat the optimization of each qubit i separately, effectively applying the desired gate $U_B(\beta)$.

3. Initialization

In order to successfully approximate a target quantum state with an RBM, a good choice of initial parameters θ in Algorithm 1 is crucial. The initial RBM state must have a nonzero overlap with the target state since gradients are proportional to the fidelity (overlap squared).

For applying $e^{-i\beta X_i}$ gates, we find that the natural choice works the best: if $\cos^2 \beta > 1/2$ then initialize the state θ as the current RBM $|\psi_\theta\rangle$ with no changes, else initialize as parameters corresponding to state $X_i|\psi_\theta\rangle$ (see Table I and Appendix A). This choice simply ensures that we start from the state that is closer to the target state given in Eq. 16.

C. Parameter count reduction

In order to simulate QAOA at depth p using the RBM framework, one needs to introduce additional hidden units in order to implement $U_C(\gamma)$ at each layer, as many as the number of edges in the underlying graph. For larger p , those extra hidden units can result in a large number of associated parameters to optimize over that are not strictly required for accurate output state approximations.

In order to keep the number of hidden units low, we employ a *compression* step at each QAOA layer (after the first). Immediately after applying the $U_C(\gamma_i)$ gate

in layer i to the RBM ψ_θ (and thereby introducing the unwanted parameters), we go through the following steps:

1. Construct a new RBM $\tilde{\psi}_\theta$.
2. Initialize $\tilde{\psi}_\theta$ to exactly represent the state $U_C\left(\sum_{j \leq i} \gamma_j\right)|+\rangle$. Doing this introduces half the number hidden units that are already present in the ψ_θ .
3. Stochastically optimize $\tilde{\psi}_\theta$ to approximate ψ_θ using Algorithm 1 with $\phi \rightarrow \psi_\theta$ and $\psi \rightarrow \tilde{\psi}_\theta$.

The optimization results in a new RBM state with fewer hidden units that closely approximates the old RBM with fidelity > 0.98 in all our tests. We then proceed to simulate the rest of the QAOA circuit and apply the same compression procedure again when the number of parameters increases again. The exact schedule of applying this procedure in context of different QAOA layers can be seen on Fig. 1.

The initialization state for the optimization was chosen as an exactly reproducible RBM state that has non-zero overlap with the target (larger) RBM. In principle, any other such state would work, but we heuristically found this one to be a reliable choice across all p values studied.

III. RESULTS

In this section we present our simulation results for 20- and 54-qubit instances of QAOA. In addition we discuss model limitations and its relation to current state-of-the-art simulations.

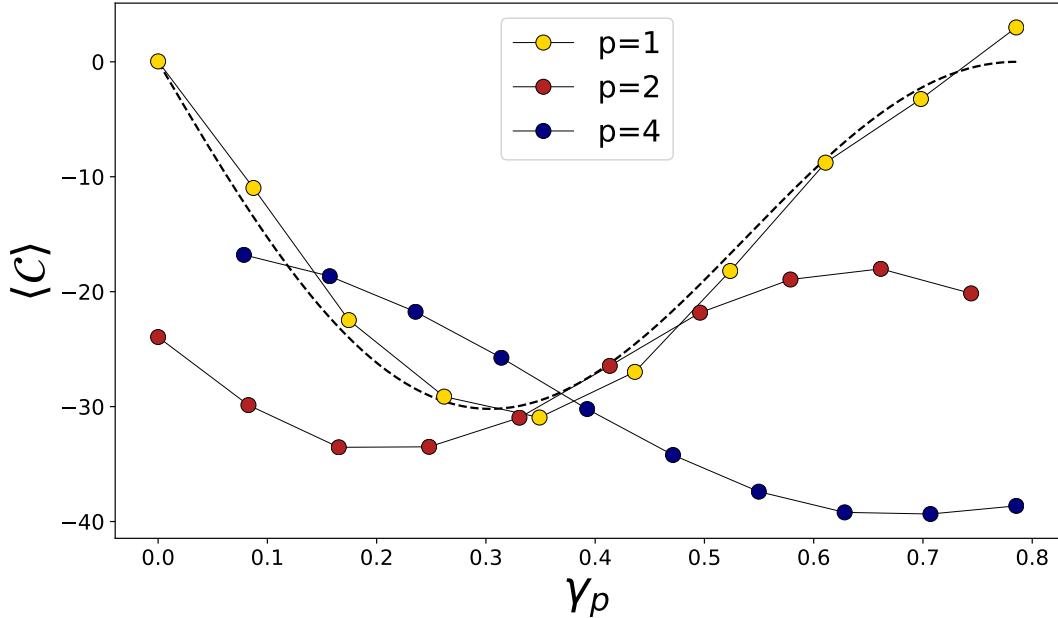


FIG. 3. Randomly generated 3-regular graphs with 54 nodes are considered at $p = 1, 2, 4$. At each p , all angles were set to optimal values for a different graph of 20 nodes, except for the final γ_p . Cost dependence along this 1D slice of the variational landscape (a higher-dimensional analogue of the leftmost panel of Fig. 2) is investigated. Data points are calculated using MCMC sampling and compared with the exact curve available through Eq. 4 at $p = 1$ (dashed curve). Error bars were calculated using bootstrap resampling but were too small to be visible on the plot. At $p = 2$, this 54-qubit simulation approximately implements 162 RZZ gates and 108 RX gates while at $p = 4$ there are 324 RZZ s and 216 RX s. Despite non-optimal angles, our model was able to capture the overall better QAOA approximation of the actual combinatorial optimum. A tight upper bound on that optimum was calculated to be $C_{\text{opt}} \lesssim -69$ by directly optimizing an RBM to represent a ground state of the cost operator in Eq. 3

A. Simulation results

We begin by studying the performance of our approach on a 20-qubit system corresponding to the MaxCut problem on a 3-regular graph of order 20. In that case, access to exact numerical wavefunctions is not yet severely restricted by the number of qubits. That makes it a suitable test-case. The results can be found on Fig. 2.

In Fig. 2, we can see that our approach reproduces variations in the cost landscape associated with different choices of QAOA angles at both $p = 1$ and $p = 2$. At $p = 1$, an exact formula (Eq. 1) is available for comparison of cost function values. We report that, at optimal angles, the overall final fidelity (overlap squared) was consistently above 0.94 for all random graph instances we simulated. Single-qubit fidelities were found to be > 0.99 almost universally. However, we find that the stochastic optimization performance seems to be sensitive to choices of QAOA variational parameters γ and β away from optimum (see Sec. III B).

In modern sum-over-Cliffords/Metropolis simulators, computational complexity grows exponentially with the number of non-Clifford gates. With the RZZ gate being a non-Clifford operation, even our 20-qubit toy example, exactly implementing 60 RZZ gates at $p = 2$, is ap-

proaching the limit of what those simulators can do [21]. In addition, that limit is greatly exceeded by the larger, 54-qubit system we study next, implementing 162 RZZ gates.

For the 54 qubit case, results can be seen on Fig. 3. We approximately reproduce the exact error curve given by Eq. 4, implementing 81 RZZ ($e^{-i\gamma Z \otimes Z}$) gates exactly and 54 RX ($e^{-i\beta X}$) gates using the described optimization method. We perform QAOA at $p = 2$ and $p = 4$ for the 54-qubit graph as well. Given that RZZ gates do not belong to the Clifford group, this simulation is the first classical implementation of QAOA on a system of this size, to the best of our knowledge, for $p = 1$, $p = 2$ and $p = 4$. Specifically at $p = 4$, we approximately implement 324 RZZ gates, greatly exceeding the capabilities of modern exact simulators. Given the favorable scaling of our approach with system size near the optimum, we conjecture that it may be used for even larger systems or larger QAOA depths p to investigate previously unknown regions of the QAOA cost landscape.

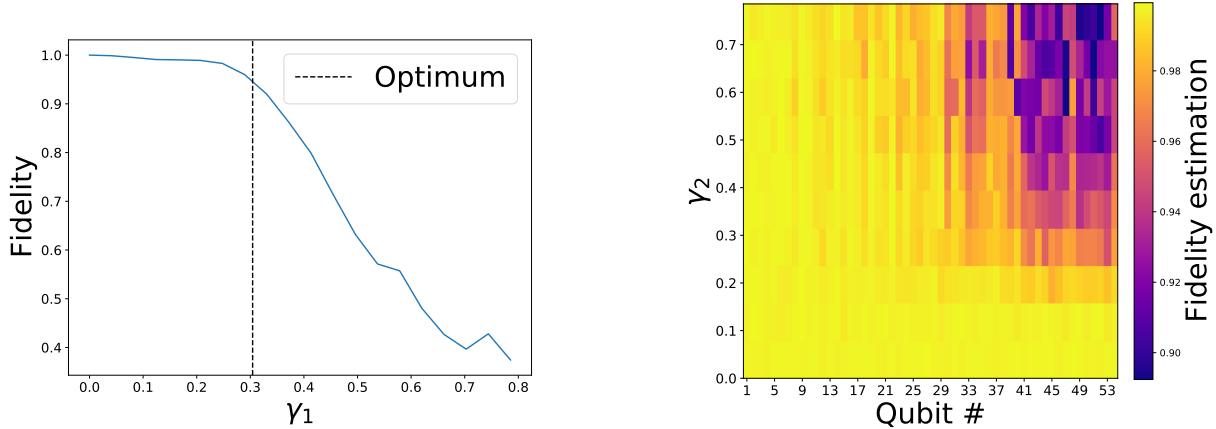


FIG. 4. **Left:** A comparison between the exact fidelity between the full RBM-ansatz wavefunction and the exact simulation results are shown for a 20 qubit system at $p = 1$. β was kept at its optimal value. We note that the fidelity begins to significantly drop approximately as γ increases beyond the optimal value. **Right:** An array of final stochastic estimations of single-qubit fidelities calculated using Eq. 15 in the course of optimizer progress. The system presented consists of 54 qubits at $p = 2$ where exact state vectors are intractable for direct comparison. A similar qubit-by-qubit trend can be noticed across all system sizes and depths p we studied.

B. Limitations

In this section we discuss our model performance for points in the QAOA cost landscape away from optimum. In general, we report that overall fidelity between the state represented by our RBM ansatz (Eq. 5) and the exact N -qubit state decreases one departs from exactly reproducible states by changing γ and β .¹ In other words, those γ and β that represent equal superpositions between two or more *RBM* states are the most difficult for our optimizer to fully capture. The situation is shown on Fig. 4.

In the case of QAOA on 3-regular graphs, we notice that the fidelity decreases as relevant parameters are increased beyond the optimum. Therefore, this model is not suitable for studying QAOA states away from the variational optimum. Based tests for small systems, we conjecture that manually increasing the number of hidden units used in the RBM ansatz may sufficiently increase its representational power to capture such non-optimal states. However, even in regions with lowest fidelities, RBM-based QAOA states have been able to approximate cost well, as can be seen in Fig. 2 and Fig. 3.

1. Complexity scaling

In this subsection, we offer scaling arguments for our method. For exact $U_C(\gamma)$ gate implementation on a k -regular graph with N qubits, $\mathcal{O}(pNk)$ sets of replacement

rules need to be implemented, for QAOA depth p . In other words, that is the minimum number of RBM hidden units to exactly represent the quantum state for arbitrary γ and $\beta = 0$, scaling linearly with depth and the number of edges in the underlying graph.

For the stochastic optimization part, the exact scaling is unknown. Therefore, we can offer only strictly heuristic arguments based on a limited number of test cases we examined. The number of MCMC samples (see Appendix D) required for reliable gradient estimations scales with QAOA depth p and qubit count N in an unknown way. Empirically, that number depends weakly on qubit count. We report that the same number of samples (of the order of 10^4) are sufficient to reproduce our results both at 20 and 54 qubits.

We also consider the minimum number of layers of independent gates, often referred to as *depth* (not to be confused with QAOA depth p) in order to make contact with existing classical simulations. In the case of QAOA, minimum depth c to implement $U_C(\gamma)$ is graph-dependent and equal to the solution of the edge coloring problem² in graph theory. Therefore, the total circuit depth (number of clock cycles required for simulation) is equal to $p(c + 1)$ because $U_B(\beta)$ can be implemented in a single layer for each p . Largest graphs considered in this work had $p = 4$ and $c = 4$ which yields a depth of 20, assuming that both *RX* and *RZZ* gates are readily available with no additional compilation overhead.

¹ By *exactly reproducible*, we mean the initial state $|+\rangle$ and all states related to it through applications of gates that can be exactly applied to the RBM ansatz. (See Appendix A)

² c is equal to the minimum number of different colors needed to mark the edges in a graph such that each no two identically colored edges share a node.

IV. CONCLUSION

In this work, we introduce a classical variational method for simulating QAOA, a hybrid quantum-classical approach for solving combinatorial optimizations with prospects of quantum speedup on near-term devices. To the best of our knowledge, this technique is the first self-contained approximate simulator based on NQS methods borrowed from many-body quantum physics, departing from the exponentially-scaling exact simulations of this class of quantum circuits.

We successfully explore previously unreachable regions in the QAOA parameter space, owing to heuristically sub-exponential complexity scaling of our method near optimal QAOA angles. Model limitations are discussed in terms of lower fidelities in quantum state reproduction away from said optimum. Because of such different area of applicability and relative low computational cost, the method is introduced as complementary to established numerical methods of classical simulation of quantum circuits.

Classical variational simulations of quantum algorithms provide a natural way to both benchmark and

understand the limitations of near-future quantum hardware. On the algorithmic side, our approach can help answer a fundamentally open question in the field, namely whether QAOA can outperform classical optimization algorithms or quantum-inspired classical algorithms based on artificial neural networks [33, 34].

Code

Our Python code is available on GitHub to reproduce the results presented in this paper.

Acknowledgements

The authors thank S. Bravyi for enlightening discussions. Numerical simulations were performed using NumPy [35], SciPy [36] and Cirq. Plots were generated using Matplotlib [37]. MM acknowledges support from the CCQ graduate fellowship in computational quantum physics. The Flatiron Institute is a division of the Simons Foundation.

-
- [1] F. Arute, K. Arya, R. Babbush, D. Bacon, J. C. Bardin, R. Barends, R. Biswas, S. Boixo, F. G. Brandao, D. A. Buell, B. Burkett, Y. Chen, Z. Chen, B. Chiaro, R. Collins, W. Courtney, A. Dunsworth, E. Farhi, B. Foxen, A. Fowler, C. Gidney, M. Giustina, R. Graff, K. Guerin, S. Habegger, M. P. Harrigan, M. J. Hartmann, A. Ho, M. Hoffmann, T. Huang, T. S. Humble, S. V. Isakov, E. Jeffrey, Z. Jiang, D. Kafri, K. Kechedzhi, J. Kelly, P. V. Klimov, S. Knysh, A. Korotkov, F. Kostritsa, D. Landhuis, M. Lindmark, E. Lucero, D. Lyakh, S. Mandrà, J. R. McClean, M. McEwen, A. Megrant, X. Mi, K. Michelsen, M. Mohseni, J. Mutus, O. Naaman, M. Neeley, C. Neill, M. Y. Niu, E. Ostby, A. Petukhov, J. C. Platt, C. Quintana, E. G. Rieffel, P. Roushan, N. C. Rubin, D. Sank, K. J. Satzinger, V. Smelyanskiy, K. J. Sung, M. D. Tervithick, A. Vainsencher, B. Villalonga, T. White, Z. J. Yao, P. Yeh, A. Zalcman, H. Neven, and J. M. Martinis, *Nature* **574**, 505 (2019).
- [2] J. Preskill, *Quantum* **2**, 79 (2018).
- [3] A. Peruzzo, J. McClean, P. Shadbolt, M. H. Yung, X. Q. Zhou, P. J. Love, A. Aspuru-Guzik, and J. L. O’Brien, *Nature Communications* **5**, 1 (2014).
- [4] E. Farhi and H. Neven, (2018), arXiv:1802.06002.
- [5] E. Farhi, J. Goldstone, and S. Gutmann, (2014), arXiv:1411.4028.
- [6] E. Grant, M. Benedetti, S. Cao, A. Hallam, J. Lockhart, V. Stojević, A. G. Green, and S. Severini, *npj Quantum Information* **4**, 1 (2018), arXiv:1804.03680.
- [7] Z. Wang, S. Hadfield, Z. Jiang, and E. G. Rieffel, *Physical Review A* **97**, 022304 (2018).
- [8] E. Farhi, J. Goldstone, and S. Gutmann, (2014), arXiv:1412.6062.
- [9] S. Lloyd, (2018), arXiv:1812.11075.
- [10] Z. Jiang, E. G. Rieffel, and Z. Wang, *Physical Review A* **95**, 062317 (2017), arXiv:1702.02577.
- [11] S. Hadfield, Z. Wang, B. O’Gorman, E. Rieffel, D. Venturelli, and R. Biswas, *Algorithms* **12**, 34 (2019).
- [12] L. Zhou, S.-T. Wang, S. Choi, H. Pichler, and M. D. Lukin, *Physical Review X* **10**, 021067 (2020).
- [13] F. Arute, K. Arya, R. Babbush, D. Bacon, J. C. Bardin, R. Barends, S. Boixo, M. Broughton, B. B. Buckley, D. A. Buell, B. Burkett, N. Bushnell, Y. Chen, Z. Chen, B. Chiaro, R. Collins, W. Courtney, S. Demura, A. Dunsworth, E. Farhi, A. Fowler, B. Foxen, C. Gidney, M. Giustina, R. Graff, S. Habegger, M. P. Harrigan, A. Ho, S. Hong, T. Huang, L. B. Ioffe, S. V. Isakov, E. Jeffrey, Z. Jiang, C. Jones, D. Kafri, K. Kechedzhi, J. Kelly, S. Kim, P. V. Klimov, A. N. Korotkov, F. Kostritsa, D. Landhuis, P. Laptev, M. Lindmark, M. Leib, E. Lucero, O. Martin, J. M. Martinis, J. R. McClean, M. McEwen, A. Megrant, X. Mi, M. Mohseni, W. Mruczkiewicz, J. Mutus, O. Naaman, M. Neeley, C. Neill, F. Neukart, H. Neven, M. Y. Niu, T. E. O’Brien, B. O’Gorman, E. Ostby, A. Petukhov, H. Puterman, C. Quintana, P. Roushan, N. C. Rubin, D. Sank, K. J. Satzinger, A. Skolik, V. Smelyanskiy, D. Strain, M. Streif, K. J. Sung, M. Szalay, A. Vainsencher, T. White, Z. J. Yao, P. Yeh, A. Zalcman, and L. Zhou, (2020), arXiv:2004.04197.
- [14] G. E. Santoro, R. Martoňák, E. Tosatti, and R. Car, *Science* **295**, 2427 (2002).
- [15] T. F. Rønnow, Z. Wang, J. Job, S. Boixo, S. V. Isakov, D. Wecker, J. M. Martinis, D. A. Lidar, and M. Troyer, *Science* **345**, 420 (2014).
- [16] G. G. Guerreschi and A. Y. Matsuura, *Scientific Reports* **9**, 1 (2019), arXiv:1812.07589.

- [17] G. Pagano, A. Bapat, P. Becker, K. S. Collins, A. De, P. W. Hess, H. B. Kaplan, A. Kyprianidis, W. L. Tan, C. Baldwin, L. T. Brady, A. Deshpande, F. Liu, S. Jordan, A. V. Gorshkov, and C. Monroe, (2019), arXiv:1906.02700.
- [18] A. Bengtsson, P. Vikstål, C. Warren, M. Svensson, X. Gu, A. F. Kockum, P. Krantz, C. Križan, D. Shiri, I.-M. Svensson, G. Tancredi, G. Johansson, P. Delsing, G. Ferrini, and J. Bylander, (2019), arXiv:1912.10495.
- [19] M. Willsch, D. Willsch, F. Jin, H. De Raedt, and K. Michielsen, *Quantum Information Processing* **19**, 1 (2020), arXiv:1907.02359.
- [20] J. S. Otterbach, R. Manenti, N. Alidoust, A. Bestwick, M. Block, B. Bloom, S. Caldwell, N. Didier, E. S. Fried, S. Hong, P. Karalekas, C. B. Osborn, A. Papageorge, E. C. Peterson, G. Prawiroatmodjo, N. Rubin, C. A. Ryan, D. Scarabelli, M. Scheer, E. A. Sete, P. Sivarajah, R. S. Smith, A. Staley, N. Tezak, W. J. Zeng, A. Hudson, B. R. Johnson, M. Reagor, M. P. da Silva, and C. Rigetti, (2017), arXiv:1712.05771.
- [21] S. Bravyi, D. Browne, P. Calpin, E. Campbell, D. Gosset, and M. Howard, *Quantum* **3**, 181 (2019), arXiv:1808.00128.
- [22] G. Carleo and M. Troyer, *Science* **355**, 602 (2017).
- [23] B. Jónsson, B. Bauer, and G. Carleo, arXiv:1808.05232 (2018), arXiv: 1808.05232.
- [24] D. P. Kingma and J. L. Ba, in *3rd International Conference on Learning Representations, ICLR 2015 - Conference Track Proceedings* (International Conference on Learning Representations, ICLR, 2015) arXiv:1412.6980.
- [25] G. E. Hinton, *Neural Computation* **14**, 1771 (2002).
- [26] G. E. Hinton and R. R. Salakhutdinov, *Science* **313**, 504 (2006).
- [27] Y. Lecun, Y. Bengio, and G. Hinton, “Deep learning,” (2015).
- [28] S. Sorella, *Physical Review Letters* **80**, 4558 (1998), arXiv:9803107 [cond-mat].
- [29] J. Stokes, J. Izaac, N. Killoran, and G. Carleo, *Quantum* **4**, 269 (2020), publisher: Verein zur Förderung des Open Access Publizierens in den Quantenwissenschaften.
- [30] S.-i. Amari, *Neural Computation* **10**, 251 (1998).
- [31] N. Metropolis, A. W. Rosenbluth, M. N. Rosenbluth, A. H. Teller, and E. Teller, *The Journal of Chemical Physics* **21**, 1087 (1953).
- [32] W. K. Hastings, *Biometrika* **57**, 97 (1970).
- [33] J. Gomes, K. A. McKiernan, P. Eastman, and V. S. Pande, arXiv:1910.10675 (2019).
- [34] T. Zhao, G. Carleo, J. Stokes, and S. Veerapaneni, arXiv:2005.04447 (2020).
- [35] S. Van Der Walt, S. C. Colbert, and G. Varoquaux, *Computing in Science and Engineering* **13**, 22 (2011).
- [36] P. Virtanen, R. Gommers, and T. E. e. a. Oliphant, *Nature Methods* **17**, 261 (2020), arXiv:1907.10121.
- [37] J. D. Hunter, *Computing in Science and Engineering* **9**, 99 (2007).
- [38] G. Carleo, F. Becca, M. Schiro, and M. Fabrizio, *Scientific Reports* **2**, 243 (2012).
- [39] M. E. J. Newman and G. T. Barkema, Oxford University Press (1999).

Appendix A: Exact gate application to Restricted Boltzmann Machines

In this appendix we enumerate the one- and two-qubit gates that can be exactly applied to the variational RBM ansatz given in Eq. 5.

1. One-qubit Pauli gates

Parameter replacement rules we use to directly apply one-qubit gates can be obtained directly by solving Eq. 6. Solutions related to Pauli gates are already listed in Table I in the main text.

a. Pauli X gate

The Pauli X_i or NOT_i gate acting on qubit i can be applied by satisfying the following system of equations:

$$\begin{aligned} \ln C + a'_i B_i &= (1 - B_i) a_i \\ b'_k + B_i W'_{ik} &= b_k + (1 - B_i) W_{ik} . \end{aligned} \tag{A1}$$

for $B_i = 0, 1$. The solution is:

$$\ln C = a_i ; \quad a'_i = -a_i ; \quad b'_k = b_k + W_{ik} ; \quad W'_{ik} = -W_{ik} , \tag{A2}$$

with all other parameters remaining unchanged.

b. *Pauli Y gate*

A similar solution can be found for the Pauli Y gate:

$$\ln C = a_i + \frac{i\pi}{2} ; \quad a'_i = -a_i + i\pi ; \quad b'_k = b_k + W_{ik} ; \quad W'_{ik} = -W_{ik} , \quad (\text{A3})$$

with all other parameters remaining unchanged as well.

c. *Pauli Z gate*

As described in the main text, one needs to solve $e^{a'_i B_i} = (-1)^{B_i} e^{a_i B_i}$. The solution is simply

$$a'_i = a_i + i\pi . \quad (\text{A4})$$

d. *Z rotations*

The Z rotation gate is given in matrix form as:

$$RZ(\varphi) = e^{-i\frac{\varphi}{2}Z} \propto \begin{pmatrix} 1 & 0 \\ 0 & e^{i\varphi} \end{pmatrix} \quad (\text{A5})$$

where the proportionality is up to a global phase factor. Similar to the Pauli Z_i gate, this gate can be implemented on qubit i by solving $e^{a'_i B_i} = e^{i\varphi B_i} e^{a_i B_i}$. The solution is simply:

$$a'_i = a_i + i\varphi , \quad (\text{A6})$$

with all other parameters besides a_i remaining unchanged. This expression reduces to the Pauli Z gate replacement rules for $\varphi = \pi$ as required.

2. Two-qubit gates

We apply two-qubit gates between qubits k and l by adding an additional hidden unit (labeled by c) to the RBM before solving Eq. 6. The extra hidden unit couples only to qubits in question, leaving all previously existing parameters unchanged. In that special case, the equation reduces to

$$e^{\Delta a_k B_k + \Delta a_l B_l} (1 + e^{W_{kc} B_k + W_{lc} B_l}) \psi_\theta(\mathcal{B}) = C \langle \mathcal{B} | \mathcal{G} | \psi_\theta \rangle . \quad (\text{A7})$$

a. *ZZ rotations*

The ZZ rotation matrix RZZ is key for being able to implement the first step in the QAOA algorithm. The definition is:

$$RZZ(\varphi) = e^{-i\frac{\varphi}{2}Z \otimes Z} \propto \begin{pmatrix} 1 & 0 & 0 & 0 \\ 0 & e^{i\varphi} & 0 & 0 \\ 0 & 0 & e^{i\varphi} & 0 \\ 0 & 0 & 0 & 1 \end{pmatrix} , \quad (\text{A8})$$

where the proportionality factor is again a global phase. The related matrix element for a RZZ_{kl} gate between qubits k and l is $\langle B'_k B'_l | RZZ_{kl}(\varphi) | B_k B_l \rangle = e^{i\varphi B_k \vee B_l}$ where \vee stands for the classical exclusive or (XOR) operation. Then, one solution to Eq. A7 reads:

$$\begin{aligned} W_{ic} &= -2\mathcal{A}(\varphi) ; & W_{jc} &= 2\mathcal{A}(\varphi) \\ a'_i &= a_i + \mathcal{A}(\varphi) ; & a'_j &= a_j - \mathcal{A}(\varphi) , \end{aligned} \quad (\text{A9})$$

where $\mathcal{A}(\varphi) = \text{Arccosh}(e^{i\varphi})$ and $C = 2$.

b. Controlled Z rotations

The controlled Z rotation matrix CRZ is defined as:

$$CRZ(\varphi) = \begin{pmatrix} 1 & 0 & 0 & 0 \\ 0 & 1 & 0 & 0 \\ 0 & 0 & 1 & 0 \\ 0 & 0 & 0 & e^{i\varphi} \end{pmatrix} , \quad (\text{A10})$$

Similar to the RZZ case, the replacement rules read:

$$\begin{aligned} W_{kc} &= -2\mathcal{A}'(\varphi) ; & W_{lc} &= 2\mathcal{A}'(\varphi) \\ a'_k &= a_k + \frac{i\varphi}{2} + \mathcal{A}'(\varphi) ; & a'_l &= a_l + \frac{i\varphi}{2} - \mathcal{A}'(\varphi) \end{aligned} \quad (\text{A11})$$

where $\mathcal{A}'(\varphi) = \text{Arccosh}(e^{-i\varphi/2})$ and $C = 2$ as well.

Appendix B: Optimization details

In this appendix we outline the optimization procedure used in this work and discuss its similarities to the time-dependent Variational Monte Carlo (t-VMC) computational techniques commonly used in many-body quantum physics.

1. The Stochastic Reconfiguration algorithm

As described in the main text, our SR optimizer finds small parameter updates Δ_k so as to approximate the action of the first-order expansion of imaginary time evolution operator associated with some hamiltonian H :

$$|\psi_{\theta+\Delta}\rangle \stackrel{!}{=} C (\mathbb{1} - \eta H) |\psi_\theta\rangle . \quad (\text{B1})$$

We use $\eta = 0.1$ throughout. In simplifying Eq. B1, one has to keep in mind that the RBM ansatz given in Eq. 5 is a holomorphic function of parameters θ and, conversely, that ψ_θ^* only depends on θ^* . Because of those facts, fidelities can be taken to independently depend on θ and θ^* .

Eq. 13 in the main text can be rewritten as:

$$\frac{\partial \mathcal{D}}{\partial \theta_l^*} = \left\langle \frac{\phi}{\psi_\theta} \right\rangle_{\psi_\theta} \left\langle \frac{\psi_\theta}{\phi} \right\rangle_\phi \left[\langle \mathcal{O}_k^* \rangle_{\psi_\theta} - \frac{\left\langle \frac{\phi}{\psi_\theta} \mathcal{O}_k^* \right\rangle_{\psi_\theta}}{\left\langle \frac{\phi}{\psi_\theta} \right\rangle_{\psi_\theta}} \right] \quad (\text{B2})$$

where \mathcal{O}_k is defined in the main text as $\mathcal{O}_k = \partial_{\theta_k} \ln \psi_\theta$.

The entire Eq. B2 is manifestly invariant to rescaling of ψ_θ and ϕ , removing the need to ever compute normalization constants.

The second step consists of multiplying the variational derivative with the inverse of the S -matrix (Eq. 14) corresponding to a stochastic estimation of a metric tensor on the hermitian parameter manifold. Thereby, the usual gradient is transformed into the natural gradient on that manifold.

However, the S -matrix is stochastically estimated and it can happen that it is singular. In order to regularize it, we replace S with $S + \epsilon \mathbb{1}$, ensuring that the resulting linear system has a unique solution. We choose $\epsilon = 10^{-3}$ throughout.

2. Relation to t-VMC

Time-dependent Variational Monte Carlo (t-VMC) [38] is a numerical technique used in many-body quantum physics to approximately capture time evolution of an arbitrary state often captured by the unitary operator e^{-iHt} associated with the system hamiltonian H . The starting point of such calculations is often almost identical to Eq. 11:

$$|\psi_{\theta(t+\Delta t)}\rangle \stackrel{!}{=} C e^{-iH\Delta t} |\psi_{\theta(t)}\rangle , \quad (\text{B3})$$

after defining an appropriate variational ansatz ψ_{θ} , usually by defining log-derivative operators \mathcal{O}_k , like in the main text of this work. By repeating the calculation outlined in the previous subsection (which in this case is equivalent to plugging into the time-dependent Schrödinger equation), one obtains the so-called optimal equations of motion:

$$\sum_l \langle \mathcal{O}_k^* \mathcal{O}_l \rangle_t^c \dot{\theta}_k(t) = -i \langle \mathcal{O}_k^* H \rangle_t^c , \quad (\text{B4})$$

where $\langle AB \rangle_t^c \equiv \langle AB \rangle_t - \langle A \rangle_t \langle B \rangle_t$ and $\langle \dots \rangle_t \equiv \langle \psi_{\theta}(t) | \dots | \psi_{\theta}(t) \rangle / \langle \psi_{\theta}(t) | \psi_{\theta}(t) \rangle$. At this point, any standard ODE solver can be employed to propagate parameters θ_k away from the initial condition after using MCMC to stochastically estimate averages $\langle \dots \rangle_t^c$ at each step. We note that t-VMC requires inverting the matrix $\langle \mathcal{O}_k^* \mathcal{O}_l \rangle_t^c$ which is analogous to the S matrix given in Eq. 14.

In the case of QAOA, one might wish to approximate the action of $U_B(\beta) = \exp(-i\beta \sum_j X_j)$ by employing t-VMC to "propagate" the relevant parameters in β instead of physical time. That approach would have the benefit of being able to apply the entire U_B gate in small $\Delta\beta$ increments instead of doing it qubit-by-qubit. Indeed, if we take Eq. B2 and set $|\phi\rangle = e^{-i\Delta\beta X_j} |\psi_{\theta}\rangle$, we obtain:

$$\frac{\partial \mathcal{D}}{\partial \theta_k^*} = \left(\frac{i}{2} \sin(2\Delta\beta) - \sin^2(\Delta\beta) \left\langle \frac{\psi_{\theta}^{X_j}}{\psi_{\theta}} \right\rangle_{\psi_{\theta}}^* \right) \left[\left\langle \mathcal{O}_k^* \frac{\psi_{\theta}^{X_j}}{\psi_{\theta}} \right\rangle_{\psi_{\theta}} - \langle \mathcal{O}_k^* \rangle_{\psi_{\theta}} \left\langle \frac{\psi_{\theta}^{X_j}}{\psi_{\theta}} \right\rangle_{\psi_{\theta}} \right] , \quad (\text{B5})$$

where $\psi_{\theta}^{X_j}(\mathcal{B}) \equiv \langle \mathcal{B} | X_j | \psi_{\theta} \rangle$. If one expands the first factor to first order in $\Delta\beta$, what is left is exactly the t -VMC parameter update one would obtain by following the t-VMC derivation from the beginning. Therefore, our method is more general than t-VMC for any individual qubit. In addition to generality, it has two other key features:

1. Fidelity $F(\phi, \psi)$ is directly used as a cost function and it is recorded at each optimization step. This provides for a more controlled environment where fidelity is explicitly optimized over rather than implicitly. We can apply as many gradient updates as needed to reach the target fidelity.
2. The computational cost of complete (approximate) application of U_B is similar between the two methods. We report that the explicit fidelity method we used in this work required approximately 30 updates per qubit while t-VMC needed 1000-2000 intermediate β points to reach similar final fidelities on 20-qubit test systems.

Appendix C: Proof of Theorem 1

The proof repeats much of what has already been done in [7]. We begin by expressing the density operator associated with the $|+\rangle$ state as

$$\rho_0 = |+\rangle\langle+| = \prod_i \frac{\mathbb{1}_i + X_i}{2} . \quad (\text{C1})$$

Then, we can express the MaxCut QAOA cost function at $p = 1$ as

$$\langle \gamma, \beta | \mathcal{C} | \gamma, \beta \rangle = \sum_{\langle k, l \rangle} \text{Tr} \left[\rho_0 U_C^\dagger(\gamma) U_B^\dagger(\beta) Z_k Z_l U_B(\beta) U_C(\gamma) \right] \quad (\text{C2})$$

In what follows, we will make repeated use of the following identities:

$$e^{i\beta X} Z e^{-i\beta X} = \cos(2\beta) Z + \sin(2\beta) Y \quad (\text{C3})$$

$$e^{-i\gamma Z \otimes Z} = \cos \gamma - i \sin \gamma Z \otimes Z \quad (\text{C4})$$

$$e^{-i\gamma Z} Y = Y e^{i\gamma Z} . \quad (\text{C5})$$

The innermost product can easily be expanded using Eq. C3 twice:

$$\begin{aligned} U_B^\dagger(\beta) Z_k Z_l U_B(\beta) &= U_B^\dagger(\beta) Z_k U_B(\beta) U_B^\dagger(\beta) Z_l U_B(\beta) = \\ &= \cos^2(2\beta) Z_k Z_l + \frac{1}{2} \sin(4\beta) (Y_k Z_l + Y_l Z_k) + \cos^2(2\beta) Y_k Y_l . \end{aligned} \quad (\text{C6})$$

The first term vanishes when averaged against ρ_0 . The second and third need to be treated separately. First we look at expressions of the form:

$$\begin{aligned} \text{Tr} [\rho_0 e^{i\gamma \mathcal{C}} Y_k Z_l e^{-i\gamma \mathcal{C}}] &= \text{Tr} \left[\rho_0 Y_k Z_l \prod_{j \in N(k)} e^{-2i\gamma Z_k Z_j} \right] = \\ &= \text{Tr} \left[\rho_0 Y_k Z_l \prod_{j \in N(k)} (\cos 2\gamma - i \sin 2\gamma Z_k Z_j) \right] , \end{aligned} \quad (\text{C7})$$

where we denoted the set of all neighbors of node k by $N(k)$ used Eq. C5 and Eq. C4. In Eq. C7, tracing out Paulis not associated to either node k or its neighbors is trivial and produces a factor of unity. Furthermore, tracing out immediate neighbors of k other than l produces a factor of $\cos^{q_k}(2\gamma)$ where $q_k + 1$ is the degree of node k . Keeping those factors aside, we are left with:

$$\text{Tr}_{kl} \left[\frac{\mathbb{1}_k + X_k}{2} \frac{\mathbb{1}_l + X_l}{2} Y_k Z_l (\cos 2\gamma - i \sin 2\gamma Z_k Z_l) \right] = \sin 2\gamma . \quad (\text{C8})$$

Therefore, the final contribution from the second term in Eq. C6 is

$$\frac{1}{2} \sin(4\beta) \text{Tr} [\rho_0 e^{i\gamma \mathcal{C}} (Y_k Z_l + Y_l Z_k) e^{-i\gamma \mathcal{C}}] = \frac{1}{2} \sin(2\gamma) \sin(4\beta) [\cos^{q_k}(2\gamma) + \cos^{q_l}(2\gamma)] \quad (\text{C9})$$

Looking at the last factor in Eq. C6, we compute:

$$\begin{aligned} \text{Tr} [\rho_0 e^{i\gamma \mathcal{C}} Y_k Y_l e^{-i\gamma \mathcal{C}}] &= \text{Tr} \left[\rho_0 Y_k Y_l \left(\prod_{\substack{j \in N(k) \\ j \neq l}} e^{-i\gamma Z_k Z_j} \right) \left(\prod_{\substack{i \in N(l) \\ i \neq k}} e^{-i\gamma Z_k Z_j} \right) e^{i\gamma Z_k Z_l} e^{-i\gamma \mathcal{C}} \right] = \\ &= \text{Tr} \left[\rho_0 Y_k Y_l \left(\prod_{\substack{j \in N(k) \\ j \neq l}} e^{-2i\gamma Z_k Z_j} \right) \left(\prod_{\substack{i \in N(l) \\ i \neq k}} e^{-2i\gamma Z_k Z_j} \right) \right] , \end{aligned} \quad (\text{C10})$$

where we separated factor in \mathcal{C} corresponding to the edge (k, l) out before using Eq. C5. In the second equality, the factor corresponding to the edge (k, l) was canceled and others were absorbed into product expressions.

Like before, operators corresponding to nodes other than k or l or their neighbors can be traced out trivially. The next step is to trace out Paulis that are neighbors of k but not l . Each of those contributes with a factor of $\cos(2\gamma)$ so we get a factor of $\cos^{q_k - \Delta_{kl}}(2\gamma)$ for node k and a corresponding factor for node l resulting in $\cos^{q_l - \Delta_{kl}}(2\gamma)$. Here, we denoted the number of common neighbors of k and l by Δ_{kl} and label their set by $CN(k, l)$ in what remains of Eq. C10:

$$\text{Tr} [\rho_0 e^{i\gamma\mathcal{C}} Y_k Y_l e^{-i\gamma\mathcal{C}}] = \cos^{q_k + q_l - 2\Delta_{kl}}(2\gamma) \text{Tr} \left[\rho'_0 Y_k Y_l \prod_{i \in CN(k, l)} (e^{-2i\gamma Z_k Z_i} e^{-2i\gamma Z_l Z_i}) \right], \quad (\text{C11})$$

where ρ'_0 is the reduced density operator. Using Eq. C4, one can trace out nodes in $CN(k, l)$ to obtain a factor of $(\cos^2 2\gamma + \sin^2 2\gamma Z_k Z_l)^{\Delta_{kl}}$. Finally, we expand that expression using the binomial theorem and interchange the trace operation with the sum. The trace in Eq. C11 becomes

$$\cos^{2\Delta_{kl}}(2\gamma) \sum_{\substack{n=0 \\ \text{odd } n}}^{\Delta_{kl}} \binom{\Delta_{kl}}{n} \tan^{2n}(2\gamma) = \frac{1}{2} (1 - \cos^{\Delta_{kl}}(4\gamma)) \quad (\text{C12})$$

Putting all of the ingredients together, we have:

$$\begin{aligned} C(\gamma, \beta) = \frac{1}{2} \sum_{\langle k, l \rangle} & \left[\sin(4\beta) \sin(2\gamma) (\cos^{q_k}(2\gamma) + \cos^{q_l}(2\gamma)) + \right. \\ & \left. + \sin^2(2\beta) \cos^{q_k + q_l - 2\Delta_{kl}}(2\gamma) (1 - \cos^{\Delta_{kl}}(4\gamma)) \right] \end{aligned} \quad (\text{C13})$$

Appendix D: Sampling details

The core difficulty with quantum computing and many-body physics is the fact that Hilbert space dimensionality rises exponentially with qubit count. That renders exact computations of expectation values for even moderately-sized system difficult. Therefore, we resort to Markov Chain Monte Carlo methods [31, 32] to importance-sample those classical bit strings \mathcal{B} that have the highest probability $|\psi(\mathcal{B})|^2$ of being measured.

To be more specific, we generate a Markov chain $\{\mathcal{B}_t\}_{t=1}^N$ of samples that are approximately distributed according to $|\psi|^2$. We use those samples to estimate the underlying distribution as the histogram of samples:

$$|\psi(\mathcal{B})|^2 \approx \frac{1}{N} \sum_{t=1}^N \delta_{\mathcal{B}\mathcal{B}_t}. \quad (\text{D1})$$

Using that representation, and assuming that $|\psi\rangle$ is normalized, we can write the expectation value of any operator \mathcal{O} as:

$$\langle \mathcal{O} \rangle_{\psi} = \langle \psi | \mathcal{O} | \psi \rangle = \sum_{\mathcal{B}} |\psi(\mathcal{B})|^2 \frac{\langle \mathcal{B} | \mathcal{O} | \psi \rangle}{\langle \mathcal{B} | \psi \rangle} \approx \frac{1}{N} \sum_{t=1}^N \frac{\langle \mathcal{B}_t | \mathcal{O} | \psi \rangle}{\langle \mathcal{B}_t | \psi \rangle} \quad (\text{D2})$$

To actually generate samples $\{\mathcal{B}_t\}_{t=1}^N$, one starts with a randomly generated bit string \mathcal{B} and sets a transition probability $T(\mathcal{B}', \mathcal{B})$. Then, the next sample \mathcal{B}' is generated from the current one according to the transition rule. The process is repeated until a sufficient number of samples is generated, tracing a "trajectory" through classical bit strings

In order to ensure convergence to the target distribution $|\psi|^2$, one usually requires two important properties from T :

- **Ergodicity**

This requires the Markov chain to have nonvanishing transition rates between any two states, given enough time steps t . We want our samples to contain points from all regions of the state space.

- **Detailed balance**

Rates of going into a state must be the same as the rate of going out of it:

$$\sum_{\mathcal{B}'} T(\mathcal{B}', \mathcal{B}) = \sum_{\mathcal{B}'} T(\mathcal{B}, \mathcal{B}') . \quad (\text{D3})$$

In other words, we cannot have states that obstruct state space trajectories, acting like sinks. In fact, we often require a stricter condition called **detailed balance**: $T(\mathcal{B}', \mathcal{B}) = T(\mathcal{B}, \mathcal{B}')$. Or, in terms of conditional probabilities:

$$T(\mathcal{B}'|\mathcal{B}) p(\mathcal{B}) \stackrel{!}{=} T(\mathcal{B}|\mathcal{B}') p(\mathcal{B}') , \quad (\text{D4})$$

where $p = |\psi|^2$ in our case. Details of these derivations can be found in standard textbooks on the subject [39].

These properties, **ergodicity** and **detailed balance** ensure that the Markov chain asymptotically converges towards the desired distribution – if we took the limit $N \rightarrow \infty$ in Eq. D1, the approximation sign would turn to equality.

To enforce detailed balance in the Metropolis-Hastings algorithm we use, $T(\mathcal{B}'|\mathcal{B})$ is broken down into "proposal" and "acceptance" factors:

$$T(\mathcal{B}'|\mathcal{B}) \equiv \underbrace{g(\mathcal{B}'|\mathcal{B})}_{\text{Proposal probability}} \times \underbrace{A(\mathcal{B}'|\mathcal{B})}_{\text{Acceptance probability}} . \quad (\text{D5})$$

That is: we first propose a new point in the state space and then decide if we accept the move. If we accept it, it gets attached at the end of the Markov chain. If not, the previous state is copied. A is typically chosen as:

$$A(\mathcal{B}'|\mathcal{B}) = \min \left\{ 1, \frac{g(\mathcal{B}|\mathcal{B}')p(\mathcal{B}')}{g(\mathcal{B}'|\mathcal{B})p(\mathcal{B})} \right\} . \quad (\text{D6})$$

From this, we can see:

$$\frac{A(\mathcal{B}'|\mathcal{B})}{A(\mathcal{B}|\mathcal{B}')} = \frac{\min \left\{ 1, \frac{g(\mathcal{B}|\mathcal{B}')p(\mathcal{B}')}{g(\mathcal{B}'|\mathcal{B})p(\mathcal{B})} \right\}}{\min \left\{ 1, \frac{g(\mathcal{B}'|\mathcal{B})p(\mathcal{B})}{g(\mathcal{B}|\mathcal{B}')p(\mathcal{B}')} \right\}} = \frac{g(\mathcal{B}|\mathcal{B}')p(\mathcal{B}')}{g(\mathcal{B}'|\mathcal{B})p(\mathcal{B})} , \quad (\text{D7})$$

which is exactly the detailed balance condition. From here, it only remains to specify $g(\mathcal{B}'|\mathcal{B})$. We use the simplest version of Metropolis-Hastings single-spin flip algorithm – at each step t randomly select a qubit B and set its value to $1 - B$ to obtain the new bit string. This choice has the added benefit of being symmetric, $g(\mathcal{B}'|\mathcal{B}) = g(\mathcal{B}|\mathcal{B}')$, cancelling some factors in Eq. D7. The complete algorithm for generating a new bitstring from the current can be found in Algorithm 2.

Algorithm 2: Metropolis-Hastings single-spin flip step

Input: Desired number of samples N , initial bit string \mathcal{B}

Result: Samples $\{\mathcal{B}_t\}_{t=1}^N \sim |\psi|^2$

choose random integer $1 \leq i \leq \text{length}(\mathcal{B})$;

$\mathcal{B}' \leftarrow \mathcal{B}$; $\mathcal{B}'_i \leftarrow 1 - \mathcal{B}'_i$;

generate $r \sim \text{Uniform}(0, 1)$;

if $|\psi(\mathcal{B}')|^2 / |\psi(\mathcal{B})|^2 > r$ **then return** \mathcal{B}' ;

else return \mathcal{B} ;
